Journal of Materials Chemistry A

RSC Publishing

PAPER

View Article Online
View Journal | View Issue



Cite this: J. Mater. Chem. A, 2013, 1, 5377

# Hydrothermally synthesized titania nanotubes as a promising electron transport medium in dye sensitized solar cells exhibiting a record efficiency of 7.6% for 1-D based devices

Jeganathan Akilavasan,[a] Kosala Wijeratne,[a] Hellio Moutinho,[b] Mowafak Al-Jassim,[b] A. R. M. Alamoud,[c] R. M. G. Rajapakse[d] and Jayasundera Bandara*[a]

Hydrothermally synthesized $TiO_2$ nanotubes (TNTs) with a diameter of approximately 10 nm and a length of 250 nm are successfully employed in dye-sensitized solar cells (DSSCs) based on N719 dye and iodide/triiodide electrolyte and exhibiting an efficiency of 7.6% at 1 sun illumination. Randomly oriented $TiO_2$ nanotubes are deposited on FTO glass by the electrophoretic deposition method, and the thickness of the TNT layer and hence the solar cell performance have been shown to depend on the deposition time and the nanotube concentration in the electrolyte solution. The highest efficiency is obtained for the solar cell fabricated with the 6-minute electrophoretically deposited $TiO_2$ film having a film thickness of ~6 μm. These pristine TNT photoelectrodes exhibit a short-circuit current density ($J_{sc}$), an open-circuit voltage ($V_{oc}$), a fill factor (FF) and an efficiency ($\eta$) of 2.4 mA $cm^{-2}$, 899 mV, 78% and 1.7%, respectively. $TiCl_4$ treatment of pristine TNT photoelectrodes enhances the $J_{sc}$, $V_{oc}$, FF and $\eta$ to 13.2 mA $cm^{-2}$, 819 mV, 70.4% and 7.6%, respectively. The $TiCl_4$ treatment is found to be vital for the enhancement of the solar cell performance of hydrothermally synthesised $TiO_2$ nanotube based devices. Enhancement of electron lifetime is noted after treatment of bare $TiO_2$ nanotubes with 0.5 M $TiCl_4$ solution. The electron transport resistance, electron lifetime and charge recombination properties of bare and $TiCl_4$ treated $TiO_2$ nanotubes are investigated by electrochemical impedance measurements. The increased performance of the DSSC fabricated with $TiCl_4$ treated TNTs is due to several factors favouring the enhancement of efficiency. These include the dye loading amount, the decrease in electron transport resistance, the increase in density of states and enhancement of light scattering.

Received 20th December 2012
Accepted 22nd February 2013

DOI: 10.1039/c3ta01576a

www.rsc.org/MaterialsA

## Introduction

DSSCs are widely recognized as a promising alternative to conventional silicon based solar cells with economically viable cost.[1,2] DSSCs contain a planar conducting electrode with a high surface area mesoporous material such as titanium dioxide to enhance light absorption of the dyes and a Pt counter electrode filled with an electrolyte containing iodide and tri-iodide ($I^-/I_3^-$) ions present in the electrolyte. When a photon is absorbed by the dye, the excited dye transfers an electron to the conduction band (CB) of the $TiO_2$ and the electron in the CB of the $TiO_2$ can diffuse to a collection electrode while the oxidized dye is regenerated by iodide. Electrons that reach the collection electrode flow through the external circuit and reduce tri-iodide to iodide at the counter electrode.[3] An efficiency of 11–12% has been reported for DSSCs based on mesoporous nanoparticles of $TiO_2$ and N719 dye with a liquid electrolyte.[4,5] The nano-crystalline semiconductor oxide layer plays a crucial role in both the physical and the chemical properties of the device while providing a path for electron transport.[3,6] One of the major drawbacks of the nano-crystalline based device is the recombination of free electrons with oxidized dye molecules and also with $I_3^-$ present in the electrolyte.[7] The recombination usually occurs at particle boundaries within the $TiO_2$ layer which is mainly due to the randomly oriented nature of the nano-crystalline particle network and poor contact between $TiO_2$ nanoparticles.[8,9] To address this issue, various methods are being investigated and among the methods being investigated for DSSC fabrication, the introduction of one dimensional (1-D) nano-structured oxide semiconductors has drawn enormous attention from every corner of the device fabrication research and the progress achieved especially in DSSCs is significant owing to realization of the potential benefits of 1-D structures such as fast electron transport and reduced charge

[a]Institute of Fundamental Studies, Hantana Road, CP20000, Kandy, Sri Lanka. E-mail: jayasundera@yahoo.com

[b]NREL, 15013 Denver West Parkway, Golden, CO 80401, USA

[c]Sustainable Energy Technology, Department of Electrical Engineering, King Saud University, Riyadh, KSA

[d]Department of Chemistry, University of Peradeniya, CP20020, Peradeniya, Sri Lanka

recombination.[8–12] In addition to the effect on electron transport, 1-D nano-structures also scatter light and enhance light harvesting.[13,14] In this respect, there has been intensive research on 1-D nano-materials such as nanotubes and nanorods during the last decade.[8,10,15–18] In comparison with spherical $TiO_2$ nanoparticles, the high aspect ratio of tubular nanotubes provides elongated direct pathways for electron travel leading to improved charge collection efficiency.[19,20] Consequently, plenty of 1-D nanostructures such as titania-nanotubes (TNTs),[9,10] titania-nanorods,[17,18] ZnO nanorods,[21] and $SnO_2$ nanorods[22] have been synthesized in both economically viable and non-viable ways. Anodization of Ti foil,[23] template assisted methods,[24] and hydrothermal methods[25] are some of the methods being employed for synthesizing 1-D $TiO_2$ nano-materials. Recently, much attention has been focused on highly ordered $TiO_2$ nanotube arrays fabricated by anodization of titanium for DSSCs due to several attractive characteristics inherent to the nanostructural architecture of these nanotube arrays. Use of $TiO_2$ nanotubes for fabrication of DSSCs reduces the number of particle boundaries within the $TiO_2$ layer and, consequently, recombination possibility. The large surface area of $TiO_2$ nanotubes is also expected to have high dye adsorption which is directly related to the photocurrent that is produced by the solar cells. However, these 1-D $TiO_2$ nano-structures failed to show considerable increase in efficiency compared to the original DSSC assembly as it was initially expected.

DSSCs have been fabricated using highly ordered $TiO_2$ nanotube arrays on FTO glass and Ti foil and efficiencies of 9.1% and 7.6% were obtained respectively.[26,27] The nanotube arrays are generally prepared by anodic oxidation of titanium or titanium films in fluoride based electrolytes.[15,28] Since the anodic oxidation process is not a cost-effective method, finding cost effective methods such as the hydrothermal method or the sol–gel process is vital for commercialization of the product. The hydrothermal process is a simple wet chemical process and it is more favourable for large-scale production of low-cost $TiO_2$ nanotubes–nanorods, compared to other methods, such as anodization[23] or surfactant-assisted templating[24] methods. An efficiency of 6.7% has been demonstrated for a DSSC fabricated with hydrothermally synthesised pristine $TiO_2$ nanotubes sensitized with N719 dye with a liquid electrolyte of $I^-/I_3^-$.[25] However, the present efficiency of hydrothermally synthesized $TiO_2$ nanotube electrodes is not comparable with the efficiency of DSSCs fabricated with $TiO_2$ nanoparticles and hence further improvement in efficiency is very important. Hence, in this investigation, the hydrothermal process was employed as an effective method for $TiO_2$ nanotube synthesis from spherical $TiO_2$ particles and photoelectrodes were fabricated on FTO glass by using high aspect ratio $TiO_2$ nanotubes by the electrophoretic method. Attempts were made to enhance the overall solar cell efficiency. We investigated the electron transport resistance, electron lifetime and charge recombination properties of bare and $TiCl_4$ treated $TiO_2$ nanotubes by the electrochemical impedance method in order to understand the significant role played by the $TiCl_4$ post-treatment method in the enhancement of the efficiency of hydrothermally synthesized $TiO_2$ nanotubes.

## Experimental

### Nanotube synthesis and fabrication of the device

Titania nanotubes were synthesized *via* hydrothermal treatment of commercially available titania nanoparticles (Degussa P25, Germany) as the starting material by using a slightly modified hydrothermal method.[25] In this method, 1 g of Degussa $TiO_2$ was well dispersed in 20 ml of 10 M NaOH (Sigma-Aldrich) aqueous solution using a magnetic stirrer for about one hour. After that, the mixture was transferred into a Teflon lined autoclave (28 ml capacity) and kept at 150 °C for 48 hours in a furnace. Then, the product was washed with distilled water several times and finally with 0.1 M HCl until a pH of 8.5 was reached. Once the required pH was achieved, the product was centrifuged at 2000 rpm and the paste was ultra-sonicated using an ultrasonicator horn (Model Sonopuls HD 2200) to get a nanotube suspension. The titania nanotube based electrode was prepared by electrophoretically depositing (EPD) the as-prepared TNT suspension onto the conducting substrate (FTO: Solaronix, 2 mm thick, sheet resistance 15 $\Omega\ \square^{-1}$). The electrolyte for EPD was prepared by mixing the TNT suspension with methanol in a 2 : 1 (v/v) ratio. The pH was adjusted to 8.5 by the addition of HCl. Methanol was added to prevent aggregation of $TiO_2$ nanotubes and current density fluctuations during EPD.[29] For EPD, a two electrode system was used with the FTO substrate as the anode and the Pt electrode as the cathode, and EPD was carried out at an optimized voltage of 40 V for different time intervals at room temperature. After deposition of $TiO_2$ nanotubes on FTO, the substrate was dried at 130 °C and sintered at 500 °C for 30 minutes. For $TiCl_4$ treatment of bare $TiO_2$ nanotube films on FTO glass, $TiO_2$ NT films were dipped in 0.5 M $TiCl_4$ aqueous solution for 30 minutes in an air-tight vessel at room temperature and excess $TiCl_4$ solution was removed by inclining the electrode and dried at room temperature followed by sintering at 500 °C for 30 minutes.[30] For dye adsorption on $TiO_2$ NT films, the photoelectrodes were soaked in a 0.3 mM solution of N719 dye for 12 h at room temperature and then washed with ethanol and dried in air. The iodide/triiodide redox couple was used as an electrolyte which consisted of tetrapropylammonium iodide (0.738 g), iodine (0.06 g), ethylene carbonate (3.6 ml) and acetonitrile (1 ml).

### Characterization of $TiO_2$ NT films and measurements of solar cell performance

XRD measurements were carried out using a powder X-ray diffraction (Bruker D8 Focus X-ray Diffractometer, with Cu K$\alpha$ radiation operating at 40 kV, scanning from $2\theta = 10$ to 70°). Scanning electron microscopy (SEM, LEO 1530 Gemini field emission scanning electron microscope FE-SEM and Hitachi SU6000 FESEM) was used to characterize the surface morphology of the thin films and powders. UV-vis absorbance spectra were measured using a Shimadzu 2450 UV-vis spectrophotometer. The current–voltage measurements of test DSSCs were performed under one sun conditions using a solar light simulator (New Port AAA solar simulator, AM 1.5 global, 100 mW $cm^{-2}$) with an active area of 0.25 $cm^2$. The intensity of

 

the light was calibrated with a standard Si-reference cell. All efficiency values reported in this work were not corrected by the spectral mismatch factor. The external quantum efficiency (EQE) experiments were performed on a Bentham PVE300 unit with a TMc 300 monochromator based IPCE with a xenon arc lamp. A calibrated type DH Si photodetector was used as a reference. EIS (Zahner Zennium Electrochemical Workstation) measurements were performed under illumination (New Port AAA solar simulator, AM 1.5 global, 100 mW $cm^{-2}$) while the cell was biased at $V_{oc}$. An AC voltage of 10 mV was superimposed on the DC voltage and the EIS experiments were performed in the frequency range of 0.1 Hz to 1 MHz. Mott–Schottky measurements were performed with a Zahner Zennium Electrochemical workstation. In all cases, a 10 mV sinusoidal excitation signal was employed to interrogate the capacitance. Capacitance was determined from two-frequency measurements at low and high frequencies. Adsorbed dye amounts were estimated after desorbing the adsorbed dye on $TiO_2$ nanotube films by using methanolic KOH solution and measuring their absorbance at 550 nm wavelength.

## Results and discussion

Efficiencies of 8.5% and 7.7% have been reported for modified composites of nanotube arrays fabricated using template assisted and anodized $TiO_2$ nanotube films ($TiO_2$ nanotubes/$TiO_2$ nanoparticles) respectively after treatment with $TiCl_4$ solution.[8,31] However, for a DSSC fabricated with a hydrothermally synthesized $TiO_2$ nanotube electrode that is treated with $TiCl_4$ and sensitized with N719 dye with a liquid electrolyte of $I^-/I_3^-$, an efficiency of only 6.7% has been reported.[25] In this investigation, we report a record efficiency of 7.6% for hydrothermally synthesised $TiO_2$ nanotube nanostructures.

The diffuse reflectance spectra of electrophoretically deposited $TiO_2$ nanotube films that were treated with 0.5 M $TiCl_4$ solution and untreated $TiO_2$ nanotube films are given in Fig. 1a. The optical properties of these compounds were probed by UV-visible diffuse reflectance spectroscopy and converted to the absorption spectra by the Kubelka–Munk method. The reflectance spectra were analyzed using the Kubelka–Munk relation to convert the reflectance into a Kubelka–Munk function (equivalent to the absorption coefficient), $F(R_\alpha)$, using the relation $F(R_\alpha) = (1 - R_\alpha)^2/2R_\alpha$, where $R_\alpha$ is the reflectance of an infinitely thick sample with respect to a reference at each wavelength. The band gap absorption edge of pure $TiO_2$ nanotubes formed by the hydrothermal method using P-25 $TiO_2$ as a precursor is determined to be 365 nm, corresponding to the band gap energy of 3.4 eV, and absorption has been blueshifted compared to P25-$TiO_2$ nanoparticles. A similar blueshift has been demonstrated for $TiO_2$ nanosheets and nanotubes.[32] Though the blueshift of absorption in $TiO_2$ nanotubes is not clear, it has been attributed to a quantum-size effect, lower dimensionality, *i.e.*, a 3D to 1D transition, the method of material preparation, crystal structure and the surface state.[32,33] It is also noteworthy that the weak shoulder at 410 nm was more clearly observed with $TiCl_4$ treated $TiO_2$ nanotubes as compared to pristine $TiO_2$ nanotubes, indicating a larger number of

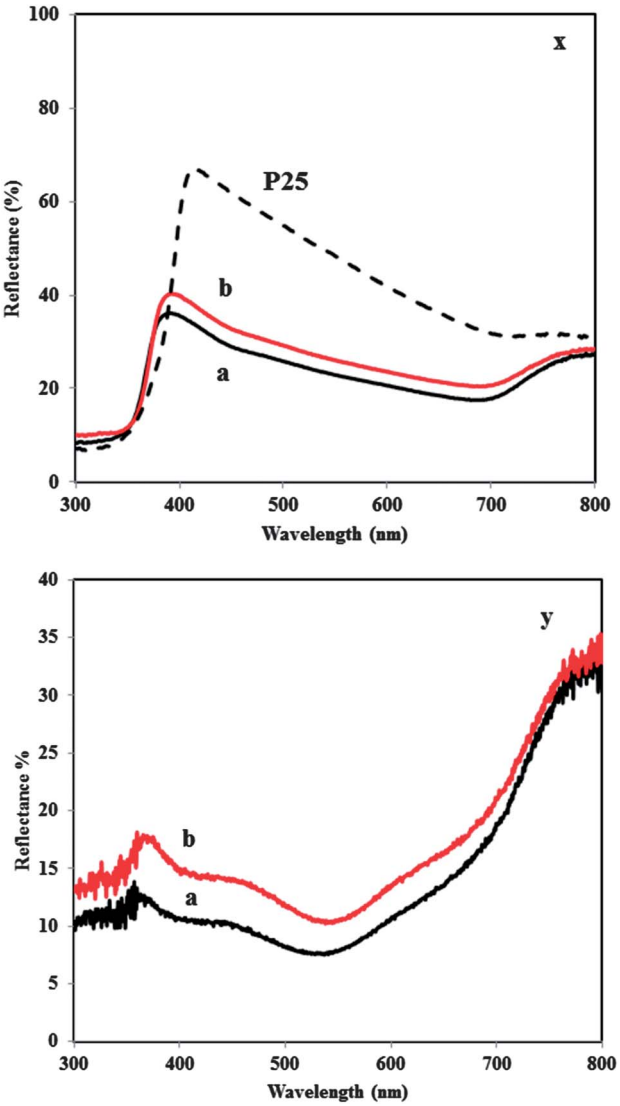


**Fig. 1** (x) Reflectance spectra of (a) pristine and (b) 0.5 M $TiCl_4$ treated $TiO_2$ nanotube films on FTO. Reflectance spectrum of P-25 $TiO_2$ is represented by a dashed line. (y) Reflectance spectra of dye treated, (a) pristine and (b) 0.5 M $TiCl_4$ treated $TiO_2$ nanotube films on FTO.

surface states available in $TiCl_4$ treated $TiO_2$ nanotubes for the electronic transition as compared to pristine $TiO_2$ nanotubes. Furthermore, as shown in Fig. 1(x), it can be said that the $TiCl_4$ treatment enhances the light scattering ability of $TiO_2$ nanotube films which in turn can enhance the solar cell performance. The reflectance spectra of N719 dye adsorbed on $TiCl_4$ treated and non-treated $TiO_2$ nanotube films are shown in Fig. 1(y). From the results presented in Fig. 1(y), enhanced dye adsorption on $TiCl_4$ treated $TiO_2$ nanotube films compared to untreated $TiO_2$ films is clearly evident and is further supported by the dye desorption analysis which gives adsorbed dye amounts of $8.98 \times 10^{-8}$ mol $cm^{-2}$ and $5.99 \times 10^{-8}$ mol $cm^{-2}$ in $TiCl_4$ treated and non-treated $TiO_2$ nanotube films, respectively.

The energy positions and donor densities of the different $TiO_2$ nanotube films were measured by Mott–Schottky plots and are given in Fig. 2. According to the capacitance data shown in

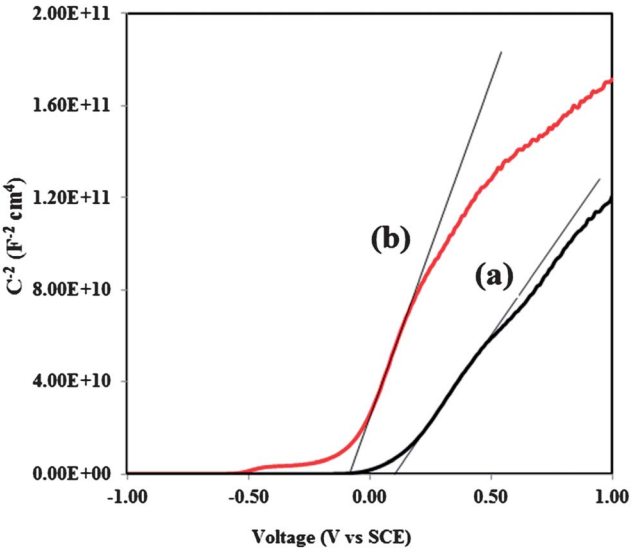


**Fig. 2** Mott–Schottky plots of (a) pristine and (b) 0.5 M $TiCl_4$ treated $TiO_2$ nanotube films on FTO.

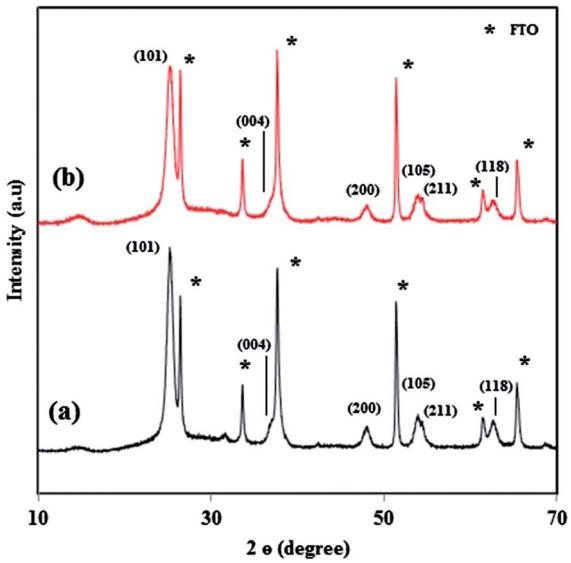


**Fig. 3** XRD patterns of (a) pristine and (b) 0.5 M $TiCl_4$ treated $TiO_2$ nanotube films.

Fig. 2, the flat-band potential $V_{fb}$ could be obtained from the $x$-intercept of the linear region of the $C^{-2}$ *vs.* $V$ curve. The measured $V_{fb}$ of $TiCl_4$ treated and non-treated $TiO_2$ nanotube films are 0.12 and −0.1 V respectively at pH 5.5 (*vs.* SCE). More importantly, $TiCl_4$ treated $TiO_2$ nanotube films showed smaller slopes of Mott–Schottky plots compared to untreated $TiO_2$ nanotube films, suggesting an increase in donor densities in $TiCl_4$ treated $TiO_2$ nanotube films. According to eqn (1) (where $e$ is the electronic charge unit, $\varepsilon_0$ is the permittivity of free space, $\varepsilon$ is the dielectric constant, $N_d$ is the dopant density ($cm^{-3}$), $V$ is the applied potential (V), and $C$ is the capacitance), the dopant density of $TiCl_4$ treated and non-treated $TiO_2$ nanotube films was calculated by using the extracted slope of the linear regions from the data shown in Fig. 2 and the calculated $N_d$ are $3.75 \times 10^{17}$ $cm^{-3}$ and $9.28 \times 10^{16}$ $cm^{-3}$, respectively.[34]

$$N_d = -\left(\frac{2}{e\varepsilon_0\varepsilon}\right)\left(\frac{d(1|C^2)}{dV}\right)^{-1} \quad (1)$$

$TiCl_4$ treatment of $TiO_2$ nanotubes increases the donor density of $TiO_2$ nanotubes by 4 times, by creating a high density of oxygen vacancies that serve as electron donors. Higher dopant density results in a large number of surface states or oxygen vacancies that are available in the nanotubes. Enhancement of surface states or oxygen vacancies in $TiO_2$ nanoparticles is known to enhance the electrical conductivity as well as the electron transfer at the interface between the semiconductor and the FTO substrate. On the other hand, it has been reported that creation of surface states may lead to higher charge recombination as these centres act as charge recombination centres, and the effect of dopant density on solar cell performance will be discussed later.

The crystal structure of the product was also characterized by the powder XRD method. Fig. 3 shows the powder XRD patterns of $TiCl_4$ treated and non-treated $TiO_2$ nanotube films annealed in air at 500 °C. The characteristic diffraction peaks of (101), (004), (200), (105) and (211) corresponding to the anatase $TiO_2$ phase are observed and agree well with the standard reported values (JCPDS 21-1272). The peak positions and their relative intensities are consistent with the standard powder diffraction pattern of anatase-$TiO_2$ and there is no preferred orientation. Diffraction patterns of the non-treated $TiO_2$ nanotube samples are similar to those of literature reported titanium oxide nanotubes.[35]

Fig. 4 shows the typical SEM images of the thin films of $TiCl_4$ treated and non-treated $TiO_2$ nanotubes on FTO after annealing at 500 °C for 1 h. The SEM image of pristine $TiO_2$ nanotubes reveals that the length and diameter of the hydrothermally synthesised titania nanotubes are ~250 nm to 10 nm, respectively. It can be clearly seen from the SEM image that the nanotubes are deposited in a randomly oriented manner, and the cross sectional image of a $TiO_2$ nanotube film (figure not shown) indicates the formation of an ~6 μm thick film for the 6-minute electrodeposited sample. In the SEM image of the 0.5 M $TiCl_4$ treated $TiO_2$ nanotube film, haziness around $TiO_2$ nanotube structures is clearly noticeable due to the deposition of a thin layer of $TiO_2$ films around $TiO_2$ nanotubes.

The current–voltage characteristics of the DSSCs based on a $TiO_2$ nanotube electrode sensitized with N719 dye with a liquid electrolyte of $I^-/I_3^-$ under AM 1.5 G illumination at a light intensity of 100 mW $cm^{-2}$ are shown in Fig. 5. DSSCs fabricated with pristine $TiO_2$ nanotubes showed a $J_{sc}$ of 2.4 mA $cm^{-2}$, a $V_{oc}$ of 899 mV, an FF of 78% and an $\eta$ of 1.7%, which are in good agreement with the reported values. The $V_{oc}$ observed in this investigation is found to be the highest reported $V_{oc}$ for hydrothermally synthesized or anodized $TiO_2$ nanotube arrays. However, for the same electrode, after treatment with 0.5 M $TiCl_4$ solution, the photoanode showed a record $J_{sc}$ of 13.2 mA $cm^{-2}$, a $V_{oc}$ of 819 mV, an FF of 70.4% and an $\eta$ of 7.6%. The corresponding IPCE spectrum shown as an inset in Fig. 5 is in good agreement with the corresponding $I$–$V$ curves. The

 

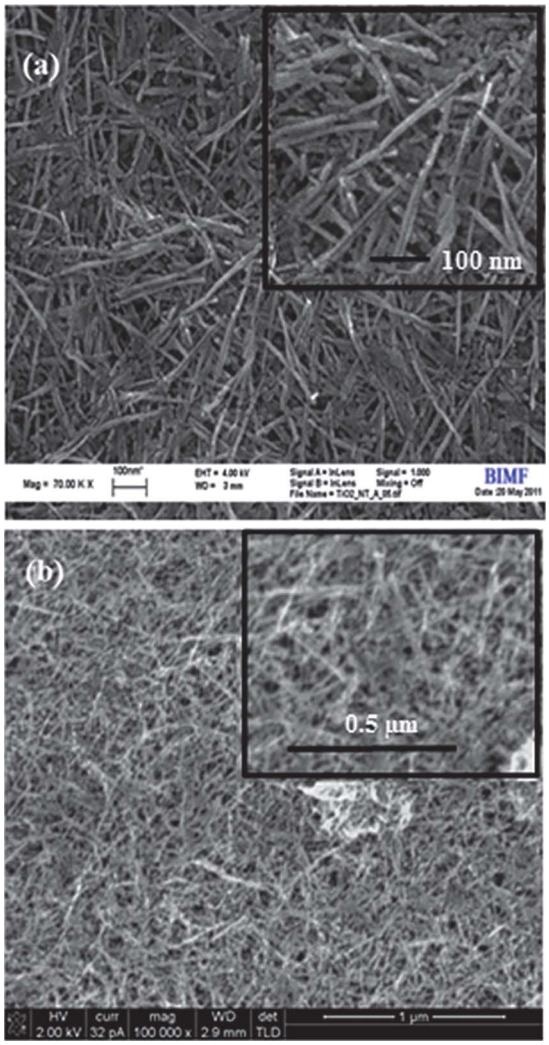


**Fig. 4** SEM images of (a) pristine and (b) 0.5 M $TiCl_4$ treated $TiO_2$ nanotube films. The inset shows the magnified image of the corresponding images.

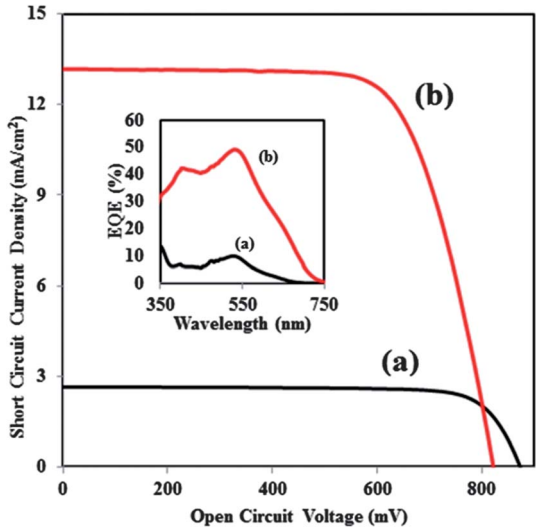


**Fig. 5** *I–V* characteristics of (a) pristine and (b) 0.5 M $TiCl_4$ treated $TiO_2$ nanotube films at 1.0 sun under 1.5 AM conditions. The inset shows the EQE measurements of (a) pristine and (b) 0.5 M $TiCl_4$ treated $TiO_2$ nanotube films.

reported $J_{sc}$, FF and $\eta$ in this investigation are the highest reported values for hydrothermally synthesized $TiO_2$ nanotube solar cells. From the results presented in Fig. 5, higher performance for the solar cells fabricated in this investigation is clearly noticeable compared to the literature reported values. The major difference here is that in this investigation, we used 0.5 M $TiCl_4$ solution for the treatment of $TiO_2$ nanotubes, whereas in the literature, ~0.04 M $TiCl_4$ solution was always used for the treatment of $TiO_2$ nanotubes.

The most striking feature of the above results is the increase in $J_{sc}$ from 2.4 mA $cm^{-2}$ to 13.2 mA $cm^{-2}$ and hence enhancement of overall solar cell efficiency from 1.7% to 7.6% after treatment of $TiO_2$ nanotubes with $TiCl_4$ solution for $TiO_2$ nanotube films of the same thickness. The increase in $J_{sc}$ could be due to several factors such as an increase in dye loading, better charge collection due to enhanced connectivity between $TiO_2$ nanotubes, enhanced light scattering or a decrease in charge recombination rates. In order to understand the higher solar cell efficiency of $TiCl_4$ treated $TiO_2$ nanotube films, we investigated and compared physical and electrical properties of both treated and untreated $TiO_2$ nanotube films by EIS, reflectance spectra and Mott–Schottky methods.

Enhanced dye adsorption has been reported to be the main reason for the observed increase in the photocurrent of the $TiCl_4$ post-treated $TiO_2$ nanoparticle films. The dye loading amounts of $TiCl_4$ treated and non-treated $TiO_2$ nanotube films having the same film thickness which were estimated by desorbing the adsorbed dye were $8.98 \times 10^{-8}$ mol $cm^{-2}$ and $5.99 \times 10^{-8}$ mol $cm^{-2}$, respectively, and the estimated BET surface areas were 235 and 121 $m^2 g^{-1}$ for $TiCl_4$ treated and non-treated $TiO_2$ nanotube films, respectively. These data clearly demonstrate the enhancement of the surface area and hence the adsorbed dye amount in $TiO_2$ nanotubes after post-treatment of $TiO_2$ nanotubes with $TiCl_4$ solution, indicating that enhanced dye adsorption on pre-treated $TiO_2$ nanotubes may be one of the reasons for enhanced $J_{sc}$. However, as shown in Fig. 5, the increase in current after post-treatment of $TiO_2$ nanotubes is 5.5 times that of the non-treated $TiO_2$ nanotubes, whereas dye adsorption results show that the treated film adsorbs 1.5 times more dye amounts than non-treated films which is not exactly correlated to the increase in the surface area. From these results, it is obvious that the increase in $J_{sc}$ is more than the increase in dye loading and hence the increase in $J_{sc}$ cannot be solely ascribed to enhanced dye loading. Hence, it indicates that other than dye loading amount, various other factors such as light scattering and electrical properties of $TiO_2$ nanotubes also contribute to the enhancement of solar cell performance. It is known that the light scattering effect within the film promotes photon capture by dye molecules leading to enhancement of short circuit current. To investigate whether the light scattering effect plays a role in enhancing the $J_{sc}$ in nanotube films, we compared the light scattering properties of the $TiCl_4$ treated and non-treated $TiO_2$ nanotube films by reflectance spectroscopy (Fig. 1). As shown in Fig. 1, $TiO_2$ nanotube films show a higher light scattering effect and the enhanced light scattering ability

of $TiO_2$ nanotube films in turn can contribute additionally to the enhancement of solar cell performance.

To further understand the higher solar cell efficiency of $TiCl_4$ treated $TiO_2$ nanotube films, we investigated the electrical properties of $TiO_2$ nanotubes by EIS and Mott–Schottky measurements. Impedance measurements of $TiO_2$ films were performed under one sun illumination at the $V_{oc}$, and under dark conditions. The Nyquist plots of these $TiO_2$ nanotube films under illumination at $V_{oc}$ are shown in Fig. 6a, while the corresponding plots under dark conditions are shown in Fig. 6b. The inset of Fig. 6a shows the enlarged Nyquist plot shown in Fig. 6a to explain the linear section of the Nyquist plot of $TiCl_4$ treated and non-treated $TiO_2$ nanotube films. The diameters of the first, second and third semicircles from the high frequency region to the low frequency region correspond to the charge transfer resistance at the counter electrode, the electron transport resistance along the TNTs and the charge transfer resistance at the working electrode (electron accumulation and recombination processes in the nanocrystalline film) and the electrolyte diffusion process ($I^-/I_3^-$ in the electrolyte) respectively. In this investigation, the third semicircle is not observed in the frequency range used.

Hence, the semicircles observed in the high frequency range in Fig. 6a could be attributed to the redox reaction at the electrolyte–Pt counter electrode interface, while the mid-frequency semicircle describes the recombination process between electrons in $TiO_2$ and the electrolyte and the short linear section at mid-frequency reflects the macroscopic electron transport resistance in $TiO_2$. The electronic parameters of the $TiO_2$ electrodes were derived by fitting the impedance data of Nyquist plots shown in Fig. 6a and b by using the equivalent circuit according to the diffusion–recombination model shown in the inset of Fig. 6a and the results are shown as a solid line in Fig. 6. Electron transport parameters such as electron transport resistance ($R_w$), charge recombination resistance ($R_k$), effective rate constant for recombination ($k_{eff} = \omega_k$), effective electron diffusion coefficient ($D_{eff}$) and lifetime ($\tau_n$) derived from the Nyquist plots of $TiCl_4$ treated and nontreated $TiO_2$ nanotube films according to the procedure demonstrated by Adachi *et al.*[20] are given in Table 1.

As shown in Fig. 6a, under illumination at $V_{oc}$, the mid-frequency semicircle of the untreated $TiO_2$ nanotube film is larger than that of the $TiCl_4$ treated $TiO_2$ nanotube film. These results indicate the improved electron generation and transport in $TiCl_4$ treated $TiO_2$ nanotubes which agrees well with the observed overall cell efficiency. Furthermore, as shown in Fig. 6b, the mid-frequency semicircle in the Nyquist plot of the untreated $TiO_2$ nanotube film is also larger than that of the $TiCl_4$ treated $TiO_2$ nanotube film, indicating a reduced charge recombination process in untreated $TiO_2$ nanotube films. Hence, from EIS results, it can be said that the $TiCl_4$ treatment enhances the charge recombination process in $TiO_2$ nanotube films. The higher $R_k$ in the untreated $TiO_2$ nanotube films which indicates diminished electron interfacial recombination is consistent with the observation of a higher FF in the cell in comparison with the $TiCl_4$ treated $TiO_2$ nanotube films.

From Table 1 it is clear that $TiCl_4$ treatment enhances the electrical conductivity. On the other hand, $TiCl_4$ treatment results in higher charge recombination between injected electrons and electron acceptors in the redox electrolyte at the $TiO_2$–electrolyte interface compared to the untreated $TiO_2$ nanotube. Despite the fact that untreated $TiO_2$ films demonstrate better resistance to the charge recombination process, the overall cell performance is inferior to that of $TiCl_4$ treated $TiO_2$ nanotube

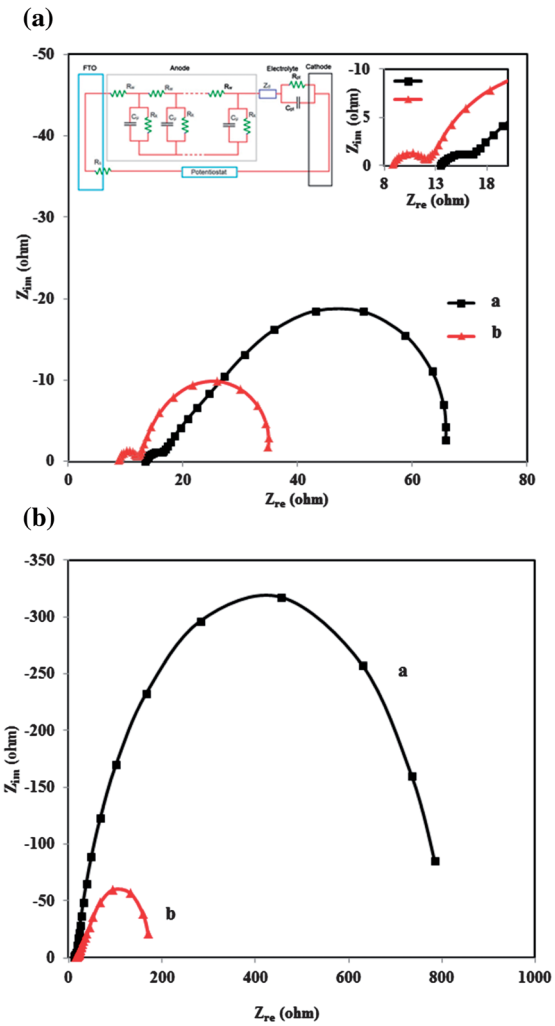


**Fig. 6** (a) EIS measurements of (a) pristine and (b) 0.5 M $TiCl_4$ treated $TiO_2$ nanotube films at 1.0 sun under 1.5 AM conditions. The inset shows the enlarged Nyquist plot to show the linear section of the plot. (b) EIS measurements of (a) pristine and (b) 0.5 M $TiCl_4$ treated $TiO_2$ nanotube films under dark conditions.

**Table 1** Electron transport properties of pristine and $TiCl_4$ treated $TiO_2$ nanotube films determined by electrochemical impedance spectroscopy

| | $R_w$ ($\Omega$ cm$^{-1}$) | $R_k$ ($\Omega$ cm$^{-1}$) | $\tau_n$ (mS) | $D_{eff}$ (m$^2$ S$^{-1}$) $\times 10^{-8}$ | $L_{eff}$ ($\mu$m) |
|---|---|---|---|---|---|
| Pristine $TiO_2$ nanotube | 2.4 | 225.5 | 30 | 4.06 | 34 |
| $TiCl_4$ treated $TiO_2$ nanotube | 1.5 | 99.7 | 54 | 4.32 | 48 |

films. As explained earlier, the EIS results shown in Fig. 6a and b for treated and untreated $TiO_2$ nanotube films under illumination and dark conditions, respectively, indicate that the electron transport resistance of $TiO_2$ nanotubes is greatly reduced by treatment with $TiCl_4$ and the same property leads to higher solar cell efficiency in treated $TiO_2$ nanorod based DSSCs. Furthermore, the calculated effective electron diffusion coefficient [$D_{eff} = (R_k/R_w)(L^2/\tau_{eff})$] and effective diffusion length [$L_{eff} = (D_{eff} \times \tau_{eff})^{1/2}$] in the treated and untreated $TiO_2$ nanotube photoanodes revealed that $D_{eff}$ and $L_{eff}$ of the $TiCl_4$ treated $TiO_2$ nanotube anode are larger than those of the untreated $TiO_2$ nanotube anode. The higher $D_{eff}$ and $L_{eff}$ for the $TiCl_4$ treated $TiO_2$ nanotube anode result in better charge collection and hence enhanced solar cell efficiency. Charge transport resistance estimated from dark EIS results (Fig. 6b) showed $R_w$ of 16.6 and 33.7 $\Omega$ $cm^{-1}$ for the $TiCl_4$ treated nanotube and untreated $TiO_2$ nanotube photoanodes respectively, further substantiating that charge transport properties of the $TiCl_4$ treated $TiO_2$ nanotube are better than those of the untreated $TiO_2$ nanotube. At this point, it is not exactly clear why electron transport resistance decreases after treatment of $TiO_2$ nanotube films with $TiCl_4$. However, previously it was shown by Mott–Schottky measurements that the $TiCl_4$ treatment of $TiO_2$ nanotubes increases the density of states of $TiO_2$ nanotubes by 4 times compared to untreated $TiO_2$ nanotubes. Enhancement of surface states or oxygen vacancies in $TiO_2$ nanoparticles is known to enhance the electrical conductivity as well as the electron transfer at the interface between the semiconductor and the FTO substrate, and hence enhanced short circuit current with the $TiCl_4$ treated $TiO_2$ nanotube films can be justified. Furthermore, according to the rate constant for electron injection, $k_{inj}$, given by Fermi's golden rule expression (eqn (2)), where $V$ is the electronic coupling between the photosensitizer and the semiconductor, $\rho(E)$ is the density-of-states (DOS) of the conduction band, and $h$ is the Planck constant, electron injection from the excited sensitizer is dependent on the $N_d$ of the conduction band.[36] As the conduction band of the pre-treated $TiO_2$ nanotube film has a relatively large density-of-states than that of the untreated $TiO_2$ film, enhanced electron injection and hence enhanced $J_{sc}$ can be expected in the pre-treated $TiO_2$ nanotube film.

$$k_{inj} = \left(\frac{4\pi^2}{h}\right)|V|^2\rho(E) \quad (2)$$

On the other hand, it has been reported that creation of surface states may lead to higher charge recombination as these centres act as charge recombination centres. Hence, a trade-off between charge recombination *vs.* charge transfer and transport rates of $TiCl_4$ treated $TiO_2$ nanotube films could lead to better solar cell performance in treated $TiO_2$ nanotube electrodes compared to untreated $TiO_2$ nanotube electrodes. Additionally, a positive shift in the conduction band edge also could contribute to the overall solar cell performance by enhancing the charge injection rates. By capacitance measurements (Fig. 2), a positive shift (by 0.22 eV) in the conduction band edge of $TiCl_4$ treated $TiO_2$ nanotubes was noted. A downward shift in the conduction band edge of $TiCl_4$ treated $TiO_2$ nanotube films when compared to untreated $TiO_2$ films results in enhanced charge injection and photocurrent due to increased driving force for the electron injection process in treated $TiO_2$ nanotubes. The observed higher $J_{sc}$ and lower $V_{oc}$ for treated $TiO_2$ nanotube films compared to untreated $TiO_2$ films confirm the contribution of the downward shift in the conduction band edge to enhancement of the overall solar cell performance of treated $TiO_2$ nanotube films. The observed lower $V_{oc}$ could be due to increased population of surface trapping sites after treatment with $TiCl_4$.

It was further noticed that the solar cell performance of electrodeposited $TiO_2$ nanotube films is highly dependent on the film thickness, and the photovoltaic performance of solar cells fabricated with nanotube $TiO_2$ films of different thicknesses that are treated with 0.5 M $TiCl_4$ solution is listed in Table 2. As the thickness of the $TiO_2$ nanotube film increases from 2.6 to 6 μm, $J_{sc}$ increases from 10.08 to 13.2 mA $cm^{-2}$ and a further increase in film thickness results in a decrease in $J_{sc}$, while $V_{oc}$ and FF show a different behaviour in that with the increase in film thickness, a decrease in $V_{oc}$ and FF is noticeable. However, the overall solar cell efficiency is found to increase with the increase in film thickness and decreases with a further increase in film thickness. The optimum solar cell

**Table 2** *I–V* characteristics of pristine and $TiCl_4$ treated $TiO_2$ nanotube films at 1.0 sun under 1.5 AM conditions

| Cell thickness (μm) | $J_{sc}$ (mA $cm^{-2}$) | $V_{oc}$ (mV) | FF (%) | $\eta$ (%) |
|---|---|---|---|---|
| 2.6 | 10.1 | 861.3 | 71.1 | 6.2 |
| 3.9 | 12.2 | 824.7 | 69.7 | 6.9 |
| 5.9 | 13.2 | 819.3 | 70.5 | 7.6 |
| 7.8 | 11.2 | 781.3 | 66.9 | 5.9 |

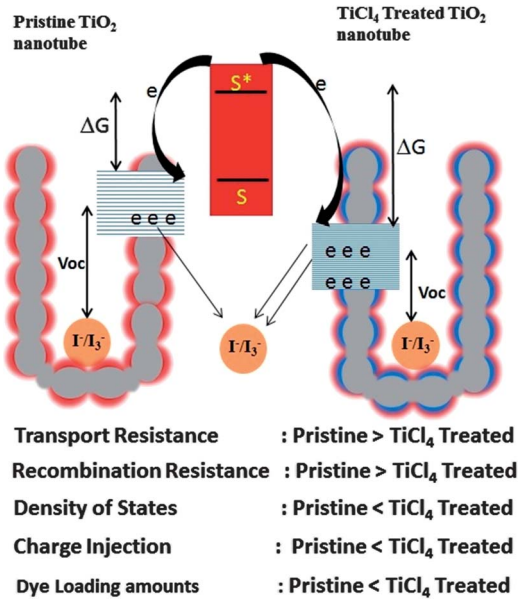


**Fig. 7** Schematic diagram of variation of electrical and physical properties of $TiO_2$ nanotubes by pre-treatment with $TiCl_4$ solution.

performance was observed for the $TiO_2$ film thickness of 6 μm. The optimum thickness can be justified due to a trade-off between the decrease in charge collection efficiency and higher dye adsorption with the increase in film thickness.

It was clearly demonstrated that efficient DSSCs can be fabricated with $TiCl_4$ treated hydrothermally synthesized $TiO_2$ nanotubes and the factors that contribute to the solar cell performance were presented in this investigation. As explained and shown schematically in Fig. 7, (a) change in density of states, (b) variation in charge transport, (c) charge recombination resistance, (d) charge injection rate, (e) shift in the conduction band edge position and (f) dye-loading amounts could be considered as important parameters for the enhancement of the solar cell performance of $TiCl_4$ treated $TiO_2$ nanotube electrodes. Though all these factors may enhance the overall solar cell efficiency, further investigation is imperative to assess the contribution of each factor to the observed enhanced solar cell efficiency of pre-treated $TiO_2$ nanotube films.

## Conclusions

The results presented in this investigation clearly suggested the enhanced efficiency of the hydrothermally synthesized $TiO_2$ nanotube electrode after treatment of $TiO_2$ nanotubes with 0.5 M $TiCl_4$. The efficiency of 7.6% is the highest ever reported for solar cell performance for the hydrothermally synthesized $TiO_2$ nanotube electrode. $TiCl_4$ treatment of hydrothermally synthesized $TiO_2$ nanotubes results in an increase in charge transport as well as charge recombination. Enhanced efficiency of the treated nanotube electrode was mainly due to enhanced charge transport, injection properties, increase in DOS and downward shift in the conduction band edge of the treated nanotube. The overall solar cell efficiency, especially short circuit current density, is highly dependent on the thickness of the $TiO_2$ nanotube film.

## Acknowledgements

Financial support (NRC 07-46) from NRC, Sri Lanka, is highly appreciated. A research grant from AvH Foundation, Germany, to purchase the electrochemical workstation is highly appreciated. JB appreciates the Visiting Professor Program of King Saud University, Riyadh, KSA.

## Notes and references

1 B. O'Regan and M. Grätzel, *Nature*, 1991, **353**, 737.
2 M. Grätzel, *Nature*, 2001, **414**, 338.
3 M. Grätzel, *J. Photochem. Photobiol., C*, 2003, **4**, 145.
4 (*a*) M. Grätzel, *J. Photochem. Photobiol., A*, 2004, **164**, 3; (*b*) A. Yella, H.-W. Lee, H. N. Tsao, C. Yi, A. K. Chandiran, M. K. Nazeeruddin, E. W.-G. Diau, C.-Y. Yeh, S. M. Zakeeruddin and M. Grätzel, *Science*, 2011, **334**, 629.
5 (*a*) C.-Y. Chen, M. Wang, J.-Y. Li, N. Pootrakulchote, L. Alibabaei, C.-h. Ngoc-le, J.-D. Decoppet, J.-H. Tsai, C. Grätzel, C.-G. Wu, S. M. Zakeeruddin and M. Grätzel, *ACS Nano*, 2009, **3**, 3103; (*b*) Y. Chiba, A. Islam, Y. Watanabe, R. Komiya, N. Koide and L. Han, *Jpn. J. Appl. Phys., Part 1*, 2006, **45**, L638.
6 F. Gao, Y. Wang, D. Shi, J. Zhang, M. Wang, X. Jing, R. Humphry-Baker, P. Wang, S. M. Zakeeruddin and M. Grätzel, *J. Am. Chem. Soc.*, 2008, **130**, 10720.
7 S. Y. Huang, G. Schlichthörl, A. J. Nozik, M. Grätzel and A. J. Frank, *J. Phys. Chem. B*, 1997, **101**, 2576.
8 M. Ye, X. Xin, C. Lin and Z. Lin, *Nano Lett.*, 2011, **11**, 3214.
9 G. K. Mor, K. Shankar, M. Paulose, O. K. Varghese and C. A. Grimes, *Nano Lett.*, 2006, **6**, 215.
10 H. Park, W.-R. Kim, H.-T. Jeong, J.-J. Lee, H.-G. Kim and W.-Y. Choi, *Sol. Energy Mater. Sol. Cells*, 2011, **95**, 184.
11 X. Wange, Y. Liu, X. Zhou, B. Li, H. Wang, W. Zhao, H. Huang, C. Liang, X. Yu, Z. Liu and H. Shen, *J. Mater. Chem.*, 2012, **22**, 17531.
12 Y. Ohsaki, N. Masaki, T. Kitamura, Y. Wada, T. Okamoto, T. Sekino, K. Niihara and S. Yanagida, *Phys. Chem. Chem. Phys.*, 2005, **7**, 4157.
13 A. Mathew, G. M. Rao and N. Munichandraiah, *Thin Solid Films*, 2012, **520**, 3581.
14 K. Zhu, N. R. Neale, A. Miedaner and A. J. Frank, *Nano Lett.*, 2007, **7**, 69.
15 H. Y. Hwang, A. A. Prabu, D. Y. Kim and K. J. Kim, *Sol. Energy*, 2011, **85**, 1551.
16 I. Tacchini, A. Ansón-Casaos, Y. Yu, M. T. Martínez and M. Lira-Cantu, *Mater. Sci. Eng., B*, 2012, **177**, 19.
17 B. Liu and E. S. Aydil, *J. Am. Chem. Soc.*, 2009, **131**, 3985.
18 J. H. Bang and P. V. Kamat, *Adv. Funct. Mater.*, 2010, **20**, 1970.
19 M. Law, L. E. Greene, J. C. Johnson, R. Saykally and P. Yang, *Nat. Mater.*, 2005, **4**, 455.
20 M. Adachi, Y. Murata, J. Takao, J. Jiu, M. Sakamoto and F. Wang, *J. Am. Chem. Soc.*, 2004, **126**, 14943.
21 I. Gonzalez-Valls and M. Lira-Cantu, *Energy Environ. Sci.*, 2009, **2**, 19.
22 K. Wijeratne, J. Akilavasan, M. Thelakkat and J. Bandara, *Electrochim. Acta*, 2012, **72**, 192.
23 C. A. Grimes, *J. Mater. Chem.*, 2007, **17**, 1451.
24 S.-I. Na, S.-S. Kim, W.-K. Hong, J.-W. Park, J. Jo, Y.-C. Nah, T. Lee and D.-Y. Kim, *Electrochim. Acta*, 2008, **53**, 2560.
25 G.-S. Kim, H.-K. Seo, V. P. Godble, Y.-S. Kim, O. B. Yang and H.-S. Shin, *Electrochem. Commun.*, 2006, **8**, 961.
26 (*a*) C.-J. Lin, W.-Y. Yu and S.-H. Chien, *J. Mater. Chem.*, 2010, **20**, 1073; (*b*) L.-L. Li, C.-Y. Tsai, H.-P. Wu, C.-C. Chen and E. W.-G. Diau, *J. Mater. Chem.*, 2010, **20**, 2753.
27 L. Sun, S. Zhang, Q. Wang and D. Zhao, *Nanosci. Nanotechnol. Lett.*, 2012, **4**, 471.
28 S. Yoriya and C. A. Grimes, *J. Mater. Chem.*, 2011, **21**, 102.
29 C. A. Grimes and G. K. Mor, in *$TiO_2$ Nanotube Arrays: Synthesis, Properties and Applications*, Springer Publications, 2009, ch. 1 and reference therein.
30 J. Bandara, K. Shankar, J. Basham, H. Wietasch, M. Paulose, O. K. Varghese, C. A. Grimes and M. Thelakkat, *Eur. Phys. J.: Appl. Phys.*, 2011, **53**, 20601.
31 E. V. A. Premalal, N. Dematage, G. R. A. Kumara, R. M. G. Rajapakse, K. Murakami and A. Konno, *Electrochim. Acta*, 2012, **63**, 375.

 

32 X. Chen and S. S. Mao, *Chem. Rev.*, 2007, **107**, 2891.
33 H.-C. Liang1, X.-Z. Li and J. Nowotny, *Solid State Phenom.*, 2010, **162**, 295.
34 R. van de Krol, A. Goossens and J. Schoonman, *J. Electrochem. Soc.*, 1997, **144**, 1723.
35 R. Liu, W.-D. Yang and L.-S. Qiang, *J. Power Sources*, 2012, **199**, 418.
36 K. Hara and H. Arakawa, in *Handbook of Photovoltaic Science and Engineering*, ed. A. Luque and S. Hegedus, Wiley Interscience, 2005, ch. 15.